Dynamic Response of an Anti-plane Shear Crack in a Functionally Graded Piezoelectric Strip

Soon Man Kwon
Department of Mechanical Design & Manufacturing, Changwon National University, 9 Sarim-dong, Changwon, Kyongnam 641-773, Korea
Kang Yong Lee*
Department of Mechanical Engineering, Yonsei University, Seoul 120-749, Korea

The dynamic response of a cracked functionally graded piezoelectric material (FGPM) under transient anti-plane shear mechanical and in-plane electrical loads is investigated in the present paper. It is assumed that the electroelastic material properties of the FGPM vary smoothly in the form of an exponential function along the thickness of the strip. The analysis is conducted on the basis of the unified (or natural) crack boundary condition which is related to the ellipsoidal crack parameters. By using the Laplace and Fourier transforms, the problem is reduced to the solutions of Fredholm integral equations of the second kind. Numerical results for the stress intensity factor and crack sliding displacement are presented to show the influences of the elliptic crack parameters, the electric field, FGPM gradation, crack length, and electromechanical coupling coefficient.

Key Words : Transient Loads, Functionally Graded Piezoelectric Material, Permeable Crack, Impermeable Crack, Unified Crack Condition, Field Intensity Factors

1. Introduction

The issue of how to impose the electrical boundary condition along the crack surfaces in piezoelectric modeling is remained still an open problem. Conventionally, two kinds of electrical boundary condition along the crack surfaces have been usually considered ; the permeable and the impermeable crack conditions. These two conditions may be regarded as the bounding cases where the permittivity of the crack is assumed to be infinite and zero, respectively. If the permeable model is used to analyze the crack instability, the applied electric load would contribute nothing to the fracture load. Such a conclusion would contradict experimental findings. This is because the presence of an electric load can either promote or retard crack growth, depending upon the magnitude and the direction of the electric load. On the other hand, based on the impermeable crack assumption, the failure strength for a piezoelectric material under the combined electric and mechanical loads has been qualitatively predicated. However, with this condition being enforced, the electric displacement intensity factor depends on the electric load, and the energy release rate is always negative only in the presence of electric loading, irrespective of its sign. This also contradicts the available experimental observations.

Recently, the concept of functionally graded materials has been extended into the studies of fracture behaviors in piezoelectric materials (Jin and Zhong, 2002 ; Li and Weng, 2002 ; Chen et al., 2003a, 2003b ; Wang, 2003 ; Shin and Kim, 2003) with the development in modern material processing technology.

The present paper investigates the problem of

* Corresponding Author,
E-mail : KYL2813@yahoo.co.kr
TEL : +82-2-2123-2813; **FAX** : +82-2-2123-2813
Department of Mechanical Engineering, Yonsei University, Seoul 120-749, Korea. (Manuscript **Received** June 30, 2003; **Revised** November 19, 2003)

a crack in a functionally graded piezoelectric ceramic strip under the combined transient anti-plane shear and in-plane electrical loading. The analysis has been conducted on the basis of the electrically unified (or natural) crack boundary condition (Xu and Rajapakse, 2001; Wang and Mai, 2003) described in Section 3, which may correct the discrepancies between the theory and experiment. It is assumed that the material properties of the functionally graded piezoelectric material (FGPM) vary continuously in terms of an exponential function along the thickness of the strip. By using integral transform techniques, the problem is first reduced to two pairs of dual integral equations and then into Fredholm integral equations of the second kind. Numerical results for the stress intensity factor (SIF) and the crack sliding displacement (CSD) are shown graphically to illustrate the influences of the elliptic crack parameters, the electric field, the FGPM gradient, the crack length, and the electromechanical coupling coefficient (EMCC).

2. Problem Statement and Governing Equations

Consider a crack of length $2a$ in an infinitely long functionally graded piezoelectric strip, which is subjected to the combined mechanical and electric transient loads as shown in Fig. 1. A set of Cartesian coordinates (x, y, z) is attached to the center of the crack for reference purposes. The FGPM poled with z-axis occupies the region $(-\infty<x<\infty,\ -h_2\le y\le h_1,\ 2h=h_1+h_2)$, and is sufficiently thick in the z-direction to allow a state of anti-plane shear. The transient shear stress, $\tau_0 H(t)$, and electric displacement, $D_0 H(t)$, are exerted on the top and bottom surfaces. Here $H(t)$ denotes the Heaviside unit step function of the time t. For convenience, we assume that the functionally graded piezoelectric strip consists of upper ($y\ge 0$ thickness h_1) and lower ($y\le 0$ thickness h_2) regions.

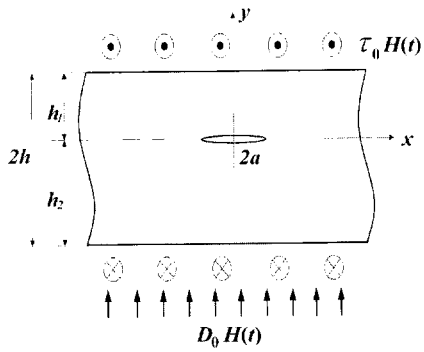

Fig. 1 Anti-plane shear crack in a functionally graded piezoelectric strip

The electroelastic boundary value problem is simplified considerably if one is only interested in the out-of-plane displacement and the in-plane electric fields, viz.

$$u_{xi}=u_{yi}=0,\ u_{zi}=w_i(x, y, t),\quad E_{xi}=E_{xi}(x, y, t),\ E_{yi}=E_{yi}(x, y, t),\ E_{zi}=0 \tag{1}$$

in which u_{ki} and $E_{ki}(k=x, y, z)$ are displacement and electric field components, respectively, and the subscripts $i=1, 2$ stand for upper and lower regions of the FGPM, respectively. The electric fields E_{xi} and E_{yi} are related to the electric potential ϕ_i by the following form:

$$E_{xi}=-\frac{\partial\phi_i}{\partial x},\ E_{yi}=-\frac{\partial\phi_i}{\partial y} \tag{2}$$

Assume that the shear modulus $c_{44}(y)$, the piezoelectric constant $e_{15}(y)$ and the dielectric permittivity $d_{11}(y)$ are the functions of y, so that the constitutive equations are written as

$$\begin{aligned}\tau_{xzi}&=c_{44}(y)\frac{\partial w_i}{\partial x}+e_{15}(y)\frac{\partial\phi_i}{\partial x}\\ \tau_{yzi}&=c_{44}(y)\frac{\partial w_i}{\partial y}+e_{15}(y)\frac{\partial\phi_i}{\partial y}\end{aligned} \tag{3}$$

$$\begin{aligned}D_{xi}&=e_{15}(y)\frac{\partial w_i}{\partial x}-d_{11}(y)\frac{\partial\phi_i}{\partial x}\\ D_{yi}&=e_{15}(y)\frac{\partial w_i}{\partial y}-d_{11}(y)\frac{\partial\phi_i}{\partial y}\end{aligned} \tag{4}$$

where (τ_{xzi}, τ_{yzi}) are the shear stress components, and (D_{xi}, D_{yi}) are the electric displacement components.

Substituting Eqs. (3) and (4) into the following equilibrium equations for the stresses and the electric displacements:

$$\frac{\partial \tau_{xzi}}{\partial x}+\frac{\partial \tau_{yzi}}{\partial y}=\rho(y)\frac{\partial^2 w_i}{\partial t^2},\ \frac{\partial D_{xi}}{\partial x}+\frac{\partial D_{yi}}{\partial y}=0 \quad (5)$$

yields

$$c_{44}(y)\nabla^2 w_i+e_{15}(y)\nabla^2\phi_i+\frac{\partial c_{44}(y)}{\partial y}\frac{\partial w_i}{\partial y}+\frac{\partial e_{15}(y)}{\partial y}\frac{\partial \phi_i}{\partial y}=\rho(y)\frac{\partial^2 w_i}{\partial t^2} \quad (6)$$

$$e_{15}(y)\nabla^2 w_i-d_{11}(y)\nabla^2\phi_i+\frac{\partial e_{15}(y)}{\partial y}\frac{\partial w_i}{\partial y}-\frac{\partial d_{11}(y)}{\partial y}\frac{\partial \phi_i}{\partial y}=0 \quad (7)$$

where $\rho(y)$ is the density of FGPM and $\nabla^2=(\partial^2/\partial x^2)+(\partial^2/\partial y^2)$ is the two dimensional Laplacian operator.

The material properties of the FGPM are supposed to be one-dimensionally dependent and described in terms of exponential functions along the strip thickness (Jin and Zhong, 2002 ; Chen et al., 2003a, 2003b ; Wang, 2003 ; Shin and Kim, 2003). But to overcome the complexity of the mathematics involved, the focus is limited on a special class of FGPMs in which the variations of these properties are in the same gradient. Therefore,

$$c_{44}(y)=c_{44}^0 e^{2\beta y},\ e_{15}(y)=e_{15}^0 e^{2\beta y}$$
$$d_{11}(y)=c_{11}^0 e^{2\beta y},\ \rho(y)=\rho_0 e^{2\beta y} \quad (8)$$

Substituting Eq. (8) into Eqs. (6) and (7), leads to

$$c_{44}^0\nabla^2 w_i+e_{15}^0\nabla^2\phi_i+2c_{44}^0\beta\frac{\partial w_i}{\partial y}+2e_{15}^0\beta\frac{\partial \phi_i}{\partial y}=\rho_0\frac{\partial^2 w_i}{\partial t^2} \quad (9)$$

$$e_{15}^0\nabla^2 w_i-d_{11}^0\nabla^2\phi_i+2e_{15}^0\beta\frac{\partial w_i}{\partial y}-2d_{11}^0\beta\frac{\partial \phi_i}{\partial y}=0 \quad (10)$$

Eqs. (9) and (10) can be decoupled by introducing the Bleustein function (Bleustein, 1968) given by $\psi_i=\phi_i-(e_{15}^0/d_{11}^0)w_i$, which reduces Eqs. (9) and (10) to

$$\nabla^2 w_i+2\beta\frac{\partial w_i}{\partial y}=\frac{1}{(C_T^0)^2}\frac{\partial^2 w_i}{\partial t^2} \quad (11)$$

$$\nabla^2\psi_i+2\beta\frac{\partial \psi_i}{\partial y}=0 \quad (12)$$

where C_T^0 is a speed of the piezoelectrically stiffened bulk shear wave, defined by

$$C_T^0=\sqrt{\frac{\mu_0}{\rho_0}}\ \text{with}\ \mu_0=\mu(0)=c_{44}^0+\frac{(e_{15}^0)^2}{d_{11}^0} \quad (13)$$

3. Solution Procedure

As usual, the crack problem can be separated into two subproblems and solved by superposition, one corresponding to the piezoelectric strip with no crack and the other corresponding to the piezoelectric strip with a crack for which the anti-plane shear stress and in-plane electric displacement applied at the crack surfaces are prescribed as the negative of those produced by the former, and the strip boundaries are also governed by appropriate conditions. From the viewpoint of fracture mechanics, the practical interest is the singular electroelastic field due to the presence of the crack. Consequently, the attention is limited to the perturbation solution for a crack.

Following the concepts of Xu and Rajapakse (2001) and Wang and Mai (2003), we introduce a newly defined electric crack condition parameter (ECCP), $D_r=D_y^c/D_0$. Here D_y^c is the normal component of the electric displacement on the crack surfaces. It is noted that D_r is zero for an impermeable crack, $(D_r)_{perm}$ for a permeable crack to be determined in Section 4, and unknown (yet-to-be-determined) for a limited permeable crack depending on the ellipsoidal crack parameters. Then the boundary conditions on the cracked plane $y=0$ can be stated as follows :

$$\tau_{yzi}(x,\ 0,\ t)=-\tau_0 H(t),\ (0\le x<a) \quad (14)$$

$$w_1(x,\ 0,\ t)=w_2(x,\ 0,\ t),\ (a\le x<\infty) \quad (15)$$

$$D_{yi}(x,\ 0,\ t)=-G_0 H(t),\ (0\le x<a) \quad (16)$$

$$\phi_1(x,\ 0,\ t)=\phi_2(x,\ 0,\ t),\ (a\le x<\infty) \quad (17)$$

where

$$G_0=D_0-D_y^c=D_0(1-D_r) \quad (18)$$

On the surfaces $y=h_1$, $y=-h_2$ and $y=0$, the traction and electric displacement boundary conditions are

$$\tau_{yz1}(x, h_1, t)=\tau_{yz2}(x, -h_2, t)=0, \ (|x|<\infty) \quad (19)$$

$$D_{y1}(x, h_1, t)=D_{y2}(x, -h_2, t)=0, \ (|x|<\infty) \quad (20)$$

$$\tau_{yz1}(x, 0, t)=\tau_{yz2}(x, 0, t), \ (a\leq x<\infty) \quad (21)$$

$$D_{y1}(x, 0, t)=D_{y2}(x, 0, t), \ (a\leq x<\infty) \quad (22)$$

Introducing the Laplace transform pair

$$f^*(p)=\int_0^\infty f(t)\, e^{-pt}dt \quad (23)$$

$$f(t)=\frac{1}{2\pi i}\int_{Br} f^*(p)\, e^{pt}dp \quad (24)$$

with Br being the Bromwich path of integration and $i=\sqrt{-1}$.

Applying first the Laplace and Fourier cosine transforms to governing equations, Eqs. (11) and (12), and then taking the inverse Fourier cosine transforms, the following results are obtained:

$$w_i^*(x, y, p)=\frac{2}{\pi}\int_0^\infty [A_{1i}(s, p)\, e^{\gamma_1 y} + A_{2i}(s, p)\, e^{\gamma_2 y}]\cos(sx)\, ds \quad (25)$$

$$\phi_i^*(x, y, p)=\frac{2}{\pi}\int_0^\infty [B_{1i}(s, p)\, e^{q_1 y} + B_{2i}(s, p)\, e^{q_2 y}]\cos(sx)\, ds \quad (26)$$

where

$$\gamma_1=-\beta+\sqrt{\gamma^2+\beta^2}, \ \gamma_2=-\beta-\sqrt{\gamma^2+\beta^2} \quad (27)$$

$$q_1=-\beta+\sqrt{s^2+\beta^2}, \ q_2=-\beta-\sqrt{s^2+\beta^2} \quad (28)$$

$$\gamma=\sqrt{s^2+(p/C_T^0)^2} \quad (29)$$

and $A_{ki}(s, p)$ and $B_{ki}(s, p)$ $(k=1, 2)$ are the unknowns to be determined.

Futhermore, it is clear that the electric potential $\phi_i^*(x, y, p)$ in the Laplace transform domain is given by

$$\phi_i^*(x, y, p) = \frac{2}{\pi}\int_0^\infty [B_{1i}(s, p)\, e^{q_1 y}+B_{2i}(s, p)\, e^{q_2 y}]\cos(sx)\, ds + \frac{e_{15}^0}{d_{11}^0}\frac{2}{\pi}\int_0^\infty [A_{1i}(s, p)\, e^{\gamma_1 y}+A_{2i}(s, p)\, e^{\gamma_2 y}]\cos(sx)\, ds \quad (30)$$

With the aid of constitutive equations, from Eqs. (3) and (4), it is not difficult to obtain the expressions for the components of the stress and the electric displacement in terms of $A_{ki}(s, p)$ and $B_{ki}(s, p)$. For instance,

$$\tau_{yzi}^*(x, y, p) = \frac{2\mu_0 e^{2\beta y}}{\pi}\int_0^\infty [\gamma_1 A_{1i}e^{\gamma_1 y}+\gamma_2 A_{2i}e^{\gamma_2 y}]\cos(sx)\, ds + \frac{2e_{15}^0 e^{2\beta y}}{\pi}\int_0^\infty [q_1 B_{1i}e^{q_1 y}+q_2 B_{2i}e^{q_2 y}]\cos(sx)\, ds \quad (31)$$

$$D_{yi}^*(x, y, p) = -\frac{2d_{11}^0 e^{2\beta y}}{\pi}\int_0^\infty [q_1 B_{1i}e^{q_1 y}+q_2 B_{2i}e^{q_2 y}]\cos(sx)\, ds \quad (32)$$

Applications of the continuity conditions on $y=0$, Eqs. (21) and (22), lead to

$$\gamma_1[A_{11}(s, p)-A_{12}(s, p)] = -\gamma_2[A_{21}(s, p)-A_{22}(s, p)]=D(s, p) \quad (33)$$

$$q_1[B_{11}(s, p)-B_{12}(s, p)] = -q_2[B_{21}(s, p)-B_{22}(s, p)]=E(s, p) \quad (34)$$

where $D(s, p)$ and $E(s, p)$ are to be determined. Also the following relationships are found from Eqs. (19) and (20) with the aid of Eqs. (33) and (34):

$$A_{11}(s, p)=-\frac{\gamma_2}{\gamma_1}A_{21}(s, p)\, e^{(\gamma_2-\gamma_1)h_1} \quad (35)$$

$$A_{21}(s, p)=-\frac{1-e^{(\gamma_2-\gamma_1)h_2}}{1-e^{(\gamma_2-\gamma_1)(h_1+h_2)}}\frac{D(s, p)}{\gamma_2} \quad (36)$$

$$B_{11}(s, p)=-\frac{q_2}{q_1}B_{21}(s, p)\, e^{(q_2-q_1)h_1} \quad (37)$$

$$B_{21}(s, p)=-\frac{1-e^{(q_2-q_1)h_2}}{1-e^{(q_2-q_1)(h_1+h_2)}}\frac{E(s, p)}{q_2} \quad (38)$$

After substituting Eqs. (33)-(38) into Eqs. (14)-(17) of the two mixed boundary conditions, we obtain the following two simultaneous dual integral equations,

$$\int_0^\infty sF_1(s, p)\, P_1(s, p)\cos(sx)\, ds = \frac{\pi}{2\mu_0 p}\left(\tau_0+\frac{e_{15}^0}{d_{11}^0}G_0\right), \ (0\leq x\leq a) \quad (39)$$

$$\int_0^\infty P_1(s, p)\cos(sx)\, ds=0, \ (a\leq x<\infty) \quad (40)$$

$$\int_0^\infty sF_2(s,\ p)\,P_2(s,\ p)\cos(sx)\,ds=-\frac{\pi}{2p}\frac{G_0}{d_{11}^0},\quad (0\le x<a) \tag{41}$$

$$\int_0^\infty\left[P_2(s,\ p)+\frac{e_{15}^0}{d_{11}^0}P_1(s,\ p)\right]\cos(sx)\,ds=0,\quad (a<x<\infty) \tag{42}$$

where

$$P_1(s,\ p)=\frac{1}{2}\left(\frac{\gamma_2-\gamma_1}{\gamma_1\gamma_2}\right)D(s,\ p)$$
$$P_2(s,\ p)=\frac{1}{2}\left(\frac{q_2-q_1}{q_1q_2}\right)E(s,\ p) \tag{43}$$

$$F_1(s,\ p)=\frac{2}{s}\left(\frac{\gamma_1\gamma_2}{\gamma_2-\gamma_1}\right)Q(s,\ p)=\frac{\gamma^2}{s\sqrt{\gamma^2+\beta^2}}Q(s,\ p) \tag{44}$$

$$F_2(s,\ p)=\frac{2}{s}\left(\frac{q_1q_2}{q_2-q_1}\right)R_M(s)=\frac{\gamma^2}{s\sqrt{\gamma^2+\beta^2}}R(s,\ p) \tag{45}$$

$$Q(s,\ p)=\frac{[1-e^{(\gamma_2-\gamma_1)h_1}][1-e^{(\gamma_2-\gamma_1)h_2}]}{1-e^{(\gamma_2-\gamma_1)(h_1+h_2)}} \tag{46}$$

$$R_M(s)=M(s,\ p)\,R(s,\ p) \tag{47}$$

$$R(s,\ p)=\frac{[1-e^{(q_2-q_1)h_1}][1-e^{(q_2-q_1)h_2}]}{M(s,\ p)[1-e^{(q_2-q_1)(h_1+h_2)}]} \tag{48}$$

$$M(s,\ p)=\frac{\left(\frac{q_2-q_1}{q_1q_2}\right)}{\left(\frac{\gamma_2-\gamma_1}{\gamma_1\gamma_2}\right)}=\left(\frac{\gamma}{s}\right)^2\frac{\sqrt{s^2+\beta^2}}{\sqrt{\gamma^2+\beta^2}} \tag{49}$$

The solution of the resulting dual integral equations (39)-(42) can be attempted by using techniques, outlined in Copson (1961). That is, if we choose $P_1(s,\ p)$ and $P_2(s,\ p)$ given by

$$P_1(s,\ p)=\frac{\pi a^2}{2\mu_0 p}\left(\tau_0+\frac{e_{15}^0}{d_{11}^0}G_0\right)\int_0^1\sqrt{\xi}\,\Omega_1^*(\xi,\ p)\,J_0(sa\xi)\,d\xi \tag{50}$$

$$P_2(s,\ p)=-\frac{\pi a^2}{2p}\frac{G_0}{d_{11}^0}\int_0^1\sqrt{\xi}\,\Omega_2^*(\xi,\ p)\,J_0(sa\xi)\,d\xi \tag{51}$$

where $J_0(\ )$ stands for the zero order Bessel function of the first kind, and $\Omega_1^*(\xi,\ p)$ and $\Omega_2^*(\xi,\ p)$ are auxiliary functions to be determined. Putting Eqs. (50) and (51) into Eqs. (39)-(42), it is easily shown that Eqs. (40) and (42) are automatically satisfied, and Eqs. (39) and (41) become the following Fredholm integral equations of the second kind:

$$\Omega_1^*(\xi,\ p)+\int_0^1\Omega_1^*(\eta,\ p)\,L_1(\xi,\ \eta,\ p)\,d\eta=\sqrt{\xi} \tag{52}$$

$$\Omega_2^*(\xi,\ p)+\int_0^1\Omega_2^*(\eta,\ p)\,L_2(\xi,\ \eta,\ p)\,d\eta=\sqrt{\xi} \tag{53}$$

with the kernels $L_1(\xi,\ \eta,\ p)$ and $L_2(\xi,\ \eta,\ p)$, given by

$$L_1(\xi,\ \eta,\ p)=\sqrt{\xi\eta}\int_0^\infty s[F_1(s/a,\ p)-1]J_0(s\xi)\,J_0(s\eta)\,ds \tag{54}$$

$$L_2(\xi,\ \eta,\ p)=\sqrt{\xi\eta}\int_0^\infty s[F_2(s/a,\ p)-1]J_0(s\xi)\,J_0(s\eta)\,ds \tag{55}$$

4. Discussions

4.1 Intensity factors and crack sliding displacement

Since of practical interest are the near tip fields around the crack, only the asymptotic fields in the neighborhood of the propagating crack will be presented here. The portions of $P_1(s,\ p)$ and $P_2(s,\ p)$ that contribute to the singular behaviors are found from the integration by part of Eqs. (50) and (51) in the forms:

$$P_1(s,\ p)=\frac{\pi\tau_0(1+\Lambda_0)a}{2\mu_0}\frac{1}{s}\frac{\Omega_1^*(1,\ p)}{p}J_1(sa)+\cdots \tag{56}$$

$$P_2(s,\ p)=-\frac{\pi D_0(1-D_r)a}{2d_{11}^0}\frac{1}{s}\frac{\Omega_2^*(1,\ p)}{p}J_1(sa)+\cdots \tag{57}$$

where

$$\Lambda_0=\lambda_0(1-D_r),\ \lambda_0=\frac{e_{15}^0}{d_{11}^0}\frac{D_0}{\tau_0} \tag{58}$$

and $J_1(\ )$ denotes the first-order Bessel function of the first kind.

Substituting Eqs. (56) and (57) into Eqs. (31) and (32), respectively, it follows that

$$K^T(t)=\lim_{x\to a^+}\sqrt{2\pi(x-a)}\,\tau_{yzi}(x,\ 0)=\tau_0\sqrt{\pi a}[(1+\Lambda_0)M_1(t)-\Lambda_0M_2(t)] \tag{59}$$

$$K^D(t)=\lim_{x\to a^+}\sqrt{2\pi(x-a)}\,D_{yi}(x,\ 0)=D_0(1-D_r)\sqrt{\pi a}M_2(t) \tag{60}$$

where

$$M_1(t)=\frac{1}{2\pi i}\int_{Br}\frac{\Omega_1^*(1,\ p)}{p}e^{pt}dp \tag{61}$$

$$M_2(t)=\frac{1}{2\pi i}\int_{Br}\frac{\Omega_2^*(1,\ p)}{p}e^{pt}dp \tag{62}$$

and $K^T(t)$ and $K^D(t)$ represent the dynamic stress intensity factor (DSIF) and the dynamic electric displacement intensity factor, respectively.

The CSD, $\Delta w(x,\ 0,\ t)$, can be easily determined by substituting Eq. (56) into the following

$$\Delta w(x,\ 0,\ t)=w_1(x,\ 0,\ t)-w_2(x,\ 0,\ t)$$
$$=\frac{4}{\pi}\int_0^\infty P_1(s,\ p)\cos(sx)\,dx, \quad (0\le x<a) \tag{63}$$

then

$$\Delta w(x,\ 0,\ t)$$
$$=\frac{2\tau_0 a}{c_{44}^0(1+k_0^2)}(1+\Lambda_0)M_1(t)\sqrt{1-\left(\frac{x}{a}\right)^2} \tag{64}$$

To obtain the conventional solutions based on the impermeable and the permeable crack assumptions, we must find the value of an unknown constant D_y^c (or D_r) which is contained in Eqs. (59) and (60). Firstly, by letting $D_r=0$ (or $\Lambda_0=\lambda_0$), the impermeable solutions are easily obtained:

$$K^T(t)=\tau_0\sqrt{\pi a}\left[(1+\lambda_0)M_1(t)-\lambda_0 M_2(t)\right] \tag{65}$$

$$K^D(t)=D_0\sqrt{\pi a}M_2(t) \tag{66}$$

$$\Delta w(x,\ 0,\ t)$$
$$=\frac{2\tau_0 a}{c_{44}^0(1+k_0^2)}(1+\lambda_0)M_1(t)\sqrt{1-\left(\frac{x}{a}\right)^2} \tag{67}$$

Next, to find the ECCP D_r satisfying the permeable assumption, an additional condition is required

$$E_{x1}(x,\ 0^+,\ t)=E_{x2}(x,\ 0^-,\ t),\ (0\le x<a) \tag{68}$$

It gives

$$(D_r)_{perm}=1-\frac{K}{\lambda_0(1-K)} \tag{69}$$

where

$$K=\frac{k_0^2}{1+k_0^2}\frac{\Omega_1^*(1,\ p)}{\Omega_2^*(1,\ p)},\ k_0=\sqrt{(e_{15}^0)^2/(c_{44}^0 d_{11}^0)} \tag{70}$$

The parameter k_0 is introduced as the EMCC in Kwon et al.(2002) that measures the strength of such coupling in a piezoelectric solid. The exact permeable solution is also given in Appendix A.

It must be addressed that the ECCP might be associated with another two parameters in an elliptical flaw, i.e. the permittivity ratio and the crack aspect ratio. The permittivity ratio κ and the aspect ratio α are defined as $\kappa=d_{11}^0/\varepsilon_a$ (d_{11}^0 and ε_a are dielectric permittivity of the ceramic and ellipse interior) and $\alpha=a/b$ (a and b are the major and minor axes of the ellipse). From the well-established result of Zhang and Tong (1996), we can determine the ECCP for an elliptical flaw of the form:

$$D_r=\frac{1+(1/\alpha)}{1+(1+k_0^2)(\kappa/\alpha)}(D_r)_{perm} \tag{71}$$

It is noted that $(D_r)_{perm}=1-k_0^2/\lambda_0$ or $\Lambda_0=k_0^2$ for the static problem. There are three limits when α approaches a sufficiently large value to describe a sharp crack. They are:

$D_r\to(D_r)_{perm}$ for a *permeable* crack when $\kappa/\alpha\to 0$

$D_r\to\dfrac{1}{1+(1+k_0^2)(\kappa/\alpha)}(D_r)_{perm}$ for a *limited permeable* crack when $\kappa/\alpha\to$ constant

$D_r\to 0$ for an *impermeable* crack when $\kappa/\alpha\to\infty$

4.2 Case studies

The solutions provided in the foregoing can now cover several special cases; as detailed below.

(*Case 1*): *Static solution.* The corresponding static solution is obtained by applying Tauberian's final value theorem (Sneddon, 1972) as follows:

$$\Omega(\xi)+\int_0^1 K(\xi,\ \eta)\Omega(\eta)\,d\eta=\sqrt{\xi} \tag{72}$$

where

$$\lim_{p\to 0}\Omega_i^*(\xi, p)=\Omega(\xi) \tag{73}$$

$$K(\xi, \eta)=\sqrt{\xi\eta}\int_0^\infty s[F_{st}(s/a)-1]J_0(s\eta)J_0(s\xi)\,ds \tag{74}$$

$$F_{st}(s)=\frac{s}{\sqrt{s^2+\beta^2}}R_M(s) \tag{75}$$

It should be pointed out in the static problem that all the results on the SIF are identical irrespective of the electric crack assumptions, but not on the EDIF.

(*Case 2*): *Purely elastic strip.* The present results are readily degenerated to those of the purely elastic strip by considering $e_{15}^0=\lambda_0=k_0=0$.

(*Case 3*): *Homogeneous solution.* To find the solutions for the homogeneous piezoelectric materials, one should let $\beta=0$. In the case,

$$F_1(s, p)=\frac{\gamma}{s}Q_h(s, p),\quad F_2(s, p)=\frac{\gamma}{s}R_h(s) \tag{76}$$

where

$$Q_h(s, p)=\frac{(1-e^{-2\gamma h_1})(1-e^{-2\gamma h_2})}{1-e^{-2\gamma(h_1+h_2)}} \tag{77}$$

$$R_h(s)=\frac{(1-e^{-2sh_1})(1-e^{-2sh_2})}{1-e^{-2s(h_1+h_2)}} \tag{78}$$

It is noted that the above dynamic and degenerated static solutions are identical to those of Shin et al.(2001a, 2001b).

(*Case 4*): *Solution of a center crack.* Considering $h_1=h_2=h$, the functions changed are as follows:

$$Q(s, p)=\tanh(\sqrt{\gamma^2+\beta^2}h) \tag{79}$$

$$R(s, p)=\tanh(\sqrt{s^2+\beta^2}h)/M(s, p) \tag{80}$$

The corresponding static problem was studied by Li and Weng (2002) with the adoption of a different form of material gradation (e.g. $c_{44}(y)=c_{44}^0(1+\alpha|y|)^k$).

(*Case 5*): *Subsurface crack parallel to the top surface of a semi-infinite piezoelectric medium.* For the case of $h_2\to\infty$, it finds that

$$Q(s, p)=1-e^{(\gamma_2-\gamma_1)h_1} \tag{81}$$

$$R(s, p)=1-e^{(q_2-q_1)h_1}/M(s, p) \tag{82}$$

If $\beta=0$ and $D_r=0$, the present results can be reduced to those of Chen and Worswick (2002).

(*Case 6*): *Solution of an infinite piezoelectric medium.* It can be easily obtained by considering $h_1, h_2\to\infty$, then

$$F_1(s, p)=\frac{\gamma^2}{s\sqrt{\gamma^2+\beta^2}},\quad F_2(s, p)=\frac{\gamma^2}{s\sqrt{\gamma^2+\beta^2}}\frac{1}{M(s, p)} \tag{83}$$

$$\lim_{p\to 0}F_1(s, p)=\lim_{p\to 0}F_2(s, p)=\frac{s}{\sqrt{s^2+\beta^2}} \tag{84}$$

for the static problem.

Eq. (84) is different from the result of Jin and Zhong (2002) for the case when the crack propagation speed $V=0$ in their results. It is due to that they employed the symmetric exponential function $e^{|\beta|y}$ instead of $e^{\beta y}$ assumed herein.

4.3 Numerical examples

In this section, numerical results for the static SIF, static CSD and DSIF are presented. In an attempt to obtain the DSIF, the inversion of Laplace transform is carried out by the numerical method developed by Miller and Guy (1966).

The uniform electric displacement load D_0 can be readily achieved in the laboratory by applying a constant potential difference across the specimen. The relationships between electric displacement and electric field at the surfaces are found from the constitutive Eqs. (3) and (4)

$$\tau_{yz}(x, h_1, t)=c_{44}(h_1)\frac{\partial w(x, h_1, t)}{\partial y}-e_{15}(h_1)E_0H(t)=\tau_0H(t) \tag{85}$$

$$D_y(x, h_1, t)=e_{15}(h_1)\frac{\partial w(x, h_1, t)}{\partial y}-d_{11}(h_1)E_0H(t)=D_0H(t) \tag{86}$$

Therefore, one can obtain

$$\lambda_0=k_0^2+e^{2\beta h_1}(1+k_0^2)\zeta_0,\quad \text{or } \zeta_0=\frac{e_{15}^0E_0}{\tau_0}=\frac{\lambda_0-k_0^2}{e^{2\beta h_1}(1+k_0^2)} \tag{87}$$

In the following numerical analysis, we will first focus on the center cracked strip (i.e. $h_1=h_2=h$) for the sake of comparison with the previous static result (Li and Weng, 2002).

Figure 2 displays the normalized static SIFs, $K^T/\tau_0\sqrt{\pi a}$, versus the crack length a/h with the variation of the gradient of material properties βa. Here $K^T=K^T(t\rightarrow\infty)$. The static SIFs increase with the increase of a/h and βa irrespective of the electrical crack condition, and the magnitude and direction of electric loads. This is in contrast to the result of Li and Weng (2002). This may result from the different assumption in the material gradation function. Also the SIF of the FGPM ($\beta a\neq 0$) is higher than that of homogeneous piezoelectric materials ($\beta a=0$). Though the SIF in the FGPM is increased, this deleterious effect can be completely offset by the high fracture toughness of the FGPM and as a result, the residual strength of the cracked FGPM may be much higher than that of the homogeneous piezoelectric ceramic (Jin and Batra, 1996).

The influences of elliptic crack parameters on the normalized CSD, $c_{44}^0\Delta w(x, 0)/(2\tau_0 a)$, in a crack position of $x/a=0.5$ are displayed in Figs. 3 and 4. In Fig. 3, a computation is performed with $\kappa=1000$, which is the order of the permittivity ratio of a ferroelectric ceramic to that of free surface. Flaws are varied in the range of elliptic aspect ratio of $100\leq\alpha\leq 3000$. The CSDs decrease or increase depending on the direction of electric field as the crack aspect ratio increases. The effect of the crack aspect ratio is smaller for

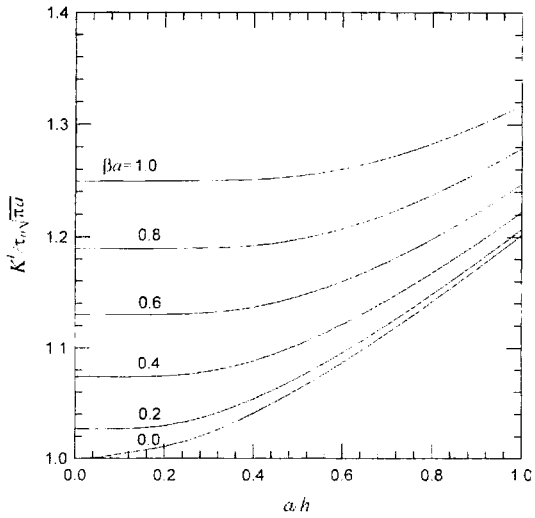

Fig. 2 $K^T/\tau_0\sqrt{\pi a}$ versus a/h with the variation of βa under static loads

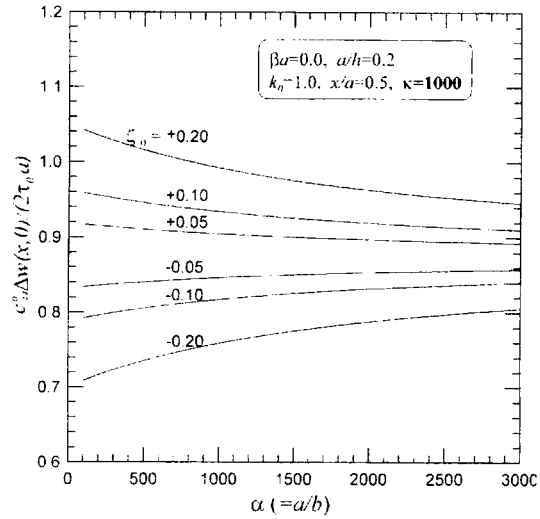

Fig. 3 The normalized CSD versus elliptic aspect ratio α in a crack position of $x/a=0.5$ with the variation of ζ_0 in a center cracked piezoelectric strip under static loads

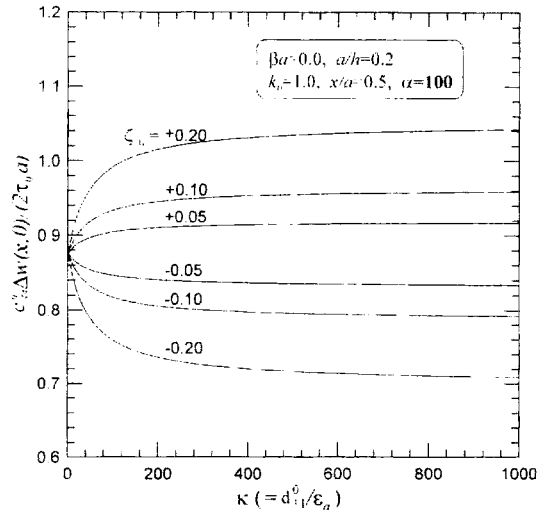

Fig. 4 The normalized CSD versus permittivity ratio κ in a crack position of $x/a=0.5$ with the variation of ζ_0 in a center cracked piezoelectric strip under static loads

the smaller electric fields. In Fig. 4, the CSD for an elliptical flaw with aspect ratio $\alpha=100$ is plotted with the variations of κ. In this case, the initial value of $\kappa=0$ corresponds to the permeable (or conducting) crack solution. The computational results show that the value of κ has the significant effect on the CSD in the small range of κ and under large electric fields. From Figs. 3 and 4, we can also observe that the impermeable solution is valid only for the problem of a non-slender hole (or cavity), whereas the permeable solution is valid only for the mathematically slit-like crack problem or for the problem of the crack whose interior is filled with a conductive medium.

Figure 5 replots the influence of the gradient of material properties βa on the normalized CSD with the variation of electric loads. The magnitudes of CSDs increase with the increase of βa. It is observed that the growth of CSD is promoted or retarded in accordance with the direction of applied electric loads; the positive electric loads enhance the CSD growth, while the negative electric loads retard it.

Figure 6 displays the influence of ζ_0 on the normalized CSD at a crack position of $x/a=0.0$ in an elliptic flaw of $\kappa=1000$ and $\alpha=1000$. As mentioned by Wang and Mai (2003), the solution based on the unified (or natural) crack boundary condition falls between those obtained from the impermeable crack and the permeable crack. The impermeable crack overestimates the effects while the permeable crack is independent of the applied electric field. However, it should be noted that according to the report of Wang and Mai (2003), the crack based on the unified crack boundary condition would never close, but the present solution shows that the crack propagation will impede in certain negative electric fields. It may be resulted from the determination of the ECCP, D_r. The shape of deformed crack relies on the finite element analysis in a research of Wang and Mai (2003), whereas the present result is based upon the closed form Eq. (71). In addition, it is observed that the effect of applied electric loads on the CSD is linear.

In Fig. 7, the effect of the EMCC k_0, a measure of the strength of the electromechanical coupling in the piezoelectric solid, is displayed. It is observed that under the unified crack condition, the magnitudes of the static CSDs increase or decrease depending upon ζ_0 with the increase of

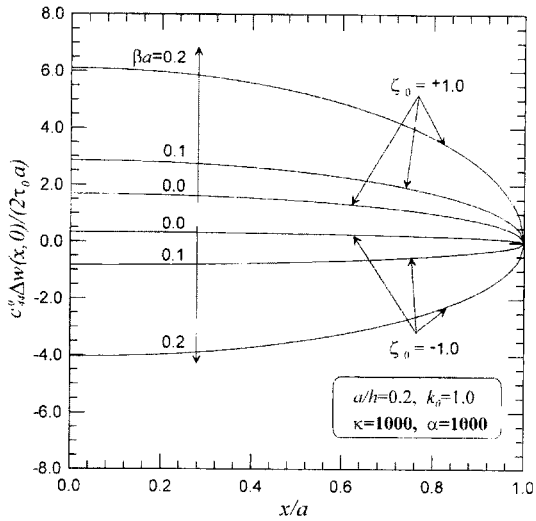

Fig. 5 The normalized CSD versus x/a with the variations of βa and ζ_0 in a center cracked functionally graded piezoelectric strip under static loads

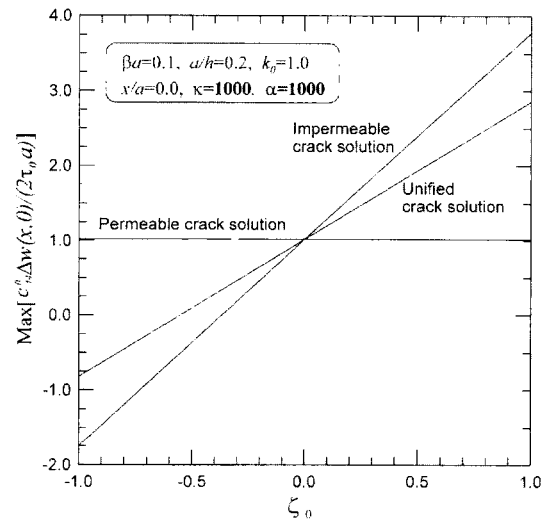

Fig. 6 The maximum normalized CSD versus ζ_0 in a center cracked functionally graded piezoelectric strip under static loads with an elliptic flaw of $\kappa=1000$ and $\alpha=1000$

k_0. However, the static CSDs based on the traditional crack conditions are constant regardless of variations in the EMCC.

Next, we investigate the effects of inertia on the DSIF of a center cracked functionally graded piezoelectric strip in Figs. 8-11.

Figure 8 depicts a plot of the normalized DSIFs $K^T(t)/\tau_0\sqrt{\pi a}$ versus the normalized time $C_T^0 t/a$, for two different values of the electric field loads ζ_0. At the early stage of impact, the DSIFs increase or decrease depending on the direction of the applied electric fields, but the trends are fully reversed after a certain normalized time, say 1.2 or so. It is also observed that the solution based on the unified crack boundary condition falls between those obtained from the impermeable crack and the permeable crack as in the static problem.

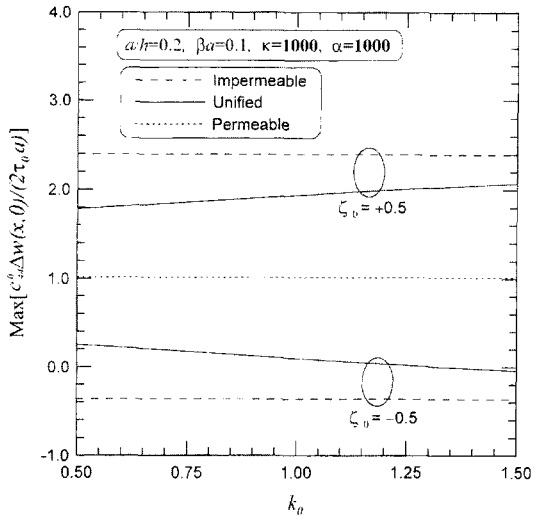

Fig. 7 The maximum normalized CSD versus k_0 with the variation of ζ_0 in a center cracked functionally graded piezoelectric strip under static loads

Figure 9 displays the influence of the gradient of material properties βa on the DSIFs. At the initial impact stage, the DSIFs decrease under the positive electric loads with the increase of βa, but increase under the negative ones. However, the trend is also reversed after a certain normalized time as in Fig. 8.

The influence of a/h on the DSIFs is shown in Fig. 10. As the crack lengths increase, the peak values of the DSIFs tend to increase.

The effect of the EMCC on the DSIFs is shown in Fig. 11. It is observed that the DSIFs decrease before a ceratin normalized time, however after the one those increase with the increase of the EMCC, irrespective of the direction of electric fields. This is more salient under the positive electric loads than under the negative ones.

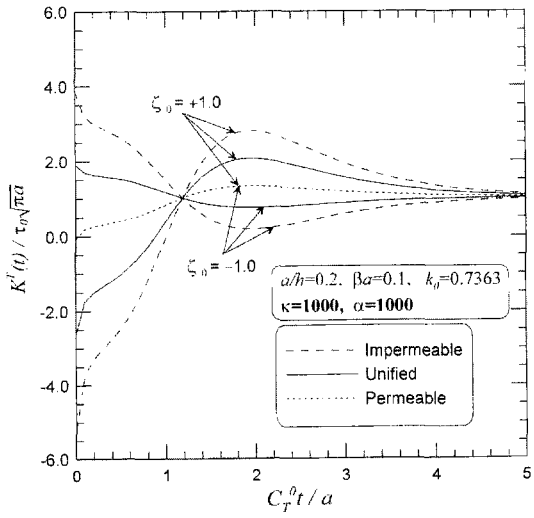

Fig. 8 $K^T(t)/\tau_0\sqrt{\pi a}$ versus $C_T^0 t/a$ with the variation of ζ_0

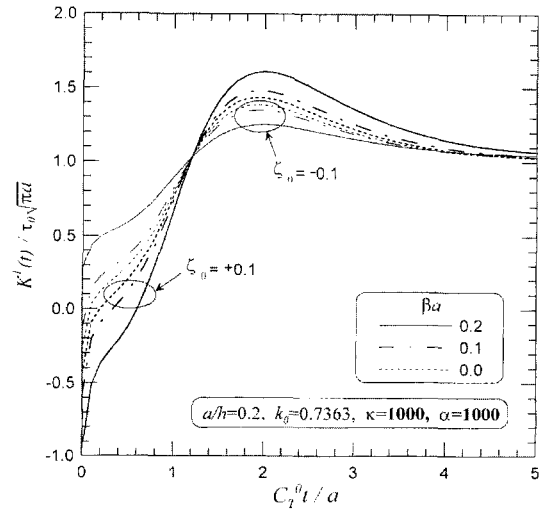

Fig. 9 $K^T(t)/\tau_0\sqrt{\pi a}$ versus $C_T^0 t/a$ with the variations of β and ζ_0

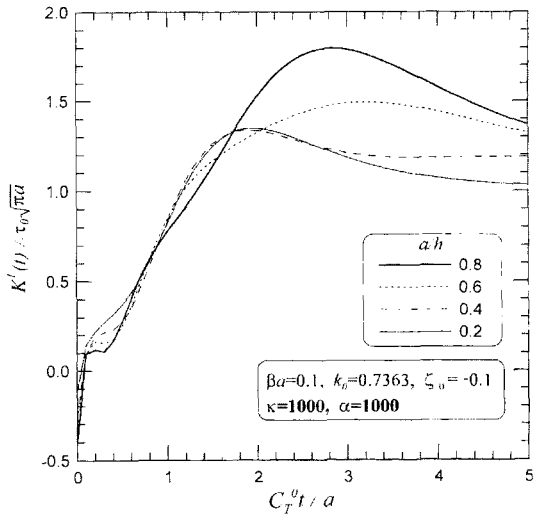

Fig. 10 $K^{I}(t)/\tau_0\sqrt{\pi a}$ versus $C_T^0 t/a$ with the variation of a/h

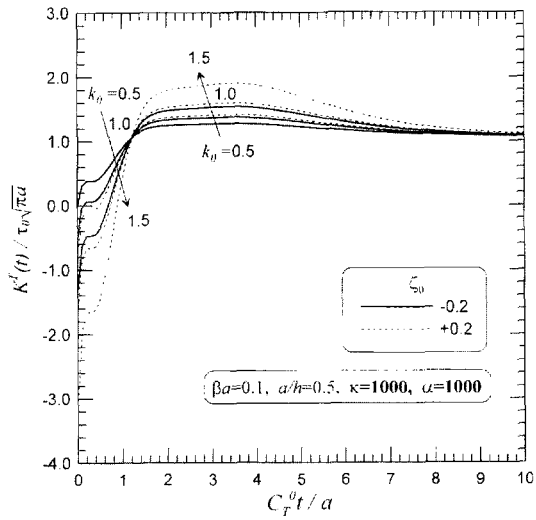

Fig. 11 $K^{I}(t)/\tau_0\sqrt{\pi a}$ versus $C_T^0 t/a$ with the variations of k_0 and ζ_0

5. Conclusions

In this paper, the transient electroelastic problem of an anti-plane shear crack in a functionally graded piezoelectric ceramic strip has been investigated by the integral transform approach. The analysis has been conducted on the basis of the unified (or natural) crack boundary condition. The dynamic intensities of stress and electric displacement have been obtained via auxiliary functions determined from the Fredholm integral equations. From the results of the current study, several conclusions have been obtained.

The present solution can describe general electrical crack conditions; especially, including the widely used impermeable one in the case of $D_\tau=0$, and the permeable one in the case of $D_\tau=(D_\tau)_{perm}$. Steeper the exponential gradients of the FGPM, higher are the SIFs. The field intensity factors are dependent on the electrical loads, the gradation of the FGPM, the crack length, and the EMCC. For the electrically permeable case, the electric impact has no contribution to the intensity factors. For the impermeable and the limited permeable cases, the crack growth under impact loads is promoted or retarded in accordance with the direction of the applied electric loads.

Appendix A

In order to obtain the exact permeable solution, one replaces Eq. (16) with the following:

$$\begin{aligned} &D_{y1}(x, 0^+, t)=D_{y2}(x, 0^-, t)\\ &\phi_1(x, 0^+, t)=\phi_2(x, 0^-, t), \quad (0\le x<a) \end{aligned} \tag{A1}$$

or

$$\begin{aligned} &D_{y1}(x, 0^+, t)=D_{y2}(x, 0^-, t)\\ &E_{x1}(x, 0^+, t)=E_{x2}(x, 0^-, t), \quad (0\le x<a) \end{aligned} \tag{A2}$$

Following the same procedure as shown in Section 3, one can find the two pairs of dual integral equations from Eqs. (14), (15), (A2) and (17) as

$$\int_0^\infty sF(s, p)P(s, p)\cos(sx)\,ds=\frac{\pi}{2}\frac{\tau_0}{p}, \quad (0\le x<a) \tag{A3}$$

$$\int_0^\infty P(s, p)\cos(sx)\,dx=0, \quad (a\le x<\infty) \tag{A4}$$

$$\int_0^\infty s\left[\left(\frac{q_2-q_1}{q_1q_2}\right)E(s, p)+\frac{e_{15}^0}{d_{11}^0}\left(\frac{\gamma_2-\gamma_1}{\gamma_1\gamma_2}\right)D(s, p)\right]\sin(sx)\,ds=0, \quad (0\le x<a) \tag{A5}$$

$$\int_0^\infty s\left[\left(\frac{q_2-q_1}{q_1q_2}\right)E(s,\ p)+\frac{e_{15}^0}{d_{11}^0}\left(\frac{\gamma_2-\gamma_1}{\gamma_1\gamma_2}\right)D(s,\ p)\right]\cos(sx)\,ds=0, \quad (0\le x<\infty) \tag{A6}$$

where

$$P(s,\ p)=\frac{c_{44}^0}{2}\left(\frac{\gamma_2-\gamma_1}{\gamma_1\gamma_2}\right)D(s,\ p) \tag{A7}$$

$$F(s,\ p)=\frac{\gamma^2}{s\sqrt{\gamma^2+\beta^2}}[(1+k_0^2)\,Q(s,\ p)-k_0^2R(s)] \tag{A8}$$

For $\beta=0$, Eq. (A8) is exactly the same as the result of Shin et al.(2001a; 2001b).

It is readily seen from Eqs. (A5) and (A6) that

$$E(s,\ p)=-\frac{e_{15}^0}{d_{11}^0}\frac{D(s,\ p)}{M(s,\ p)} \tag{A9}$$

With the aid of the Copson's method in the above Eqs. (A3) and (A4), we finally obtain a Fredholm integral equation of the second kind of the form :

$$\Omega^*(\xi,\ p)+\int_0^1\Omega^*(\eta,\ p)\,L(\xi,\ \eta,\ p)\,d\eta=\sqrt{\xi} \tag{A10}$$

where

$$L(\xi,\ \eta,\ p)=\sqrt{\xi\eta}\int_0^\infty s[F(s/a,\ p)-1]J_0(s\xi)\,J_0(s\eta)\,ds \tag{A11}$$

For the case when the uniform stress $\tau_0H(t)$ and the uniform electric displacement $D_0H(t)$ are applied at $y=h_1$ and $-h_2$, two field intensity factors and CSD are given as

$$K^T(t)=\tau_0\sqrt{\pi a}M(t) \tag{A12}$$

$$K^D(t)=\frac{e_{15}^0}{c_{44}^0}\tau_0\sqrt{\pi a}M(t)=e_{15}^0K^T(t)/c_{44}^0 \tag{A13}$$

$$\Delta w(x,\ 0,\ t)=\frac{2\tau_0 a}{c_{44}^0}M(t)\sqrt{1-\left(\frac{x}{a}\right)^2} \tag{A14}$$

where

$$M(t)=\frac{1}{2\pi i}\int_{Br}\frac{\Omega^*(1,\ p)}{p}e^{pt}dp \tag{A15}$$

References

Bleustein, J. L., 1968, "A New Surface Wave in Piezoelectric Materials," *Applied Physics Letters*, Vol. 13, pp. 412~413.

Chen, J., Liu, Z. X. and Zou, Z. Z., 2003a, "Electromechanical Impact of a Crack in a Functionally Graded Piezoelectric Medium," *Theoretical and Applied Fracture Mechanics*, Vol. 39, pp. 47~60.

Chen, J., Liu, Z. X. and Zou, Z. Z., 2003b, "Dynamic Response of a Crack in a Functionally Graded Interface of Two Dissimilar Piezoelectric Half-planes," *Archive of Applied Mechanics*, Vol. 72, pp. 686~696.

Chen, Z. T. and Worswick, M. J., 2002, "Dynamic Fracture Behavior of a Cracked Piezoelectric Half Space under Anti-plane Mechanical and In-plane Electrical Impact," *Archive of Applied Mechanics*, Vol. 72, pp. 1~12.

Copson, E. T., 1961, "On Certain Dual Integral Equations," *Proceedings of the Glasgow Mathematical Association*, Vol. 5, pp. 19~24.

Jin, Z. -H. and Batra, R. C., 1996, "Some Basic Fracture Mechanics Concepts in Functionally Graded Materials," *Journal of the Mechanics and Physics of Solids*, Vol. 44, pp. 1221~1235.

Jin, B. and Zhong, Z., 2002, "A Moving Mode-III Crack in Functionally Graded Piezoelectric Material : Permeable Problem," *Mechanics Research Communications*, Vol. 29, pp. 217~224.

Kwon, S. M., Son, M. S. and Lee, K. Y., 2002, "Transient Behavior in a Cracked Piezoelectric Layered Composite : Anti-plane Problem," *Mechanics of Materials*, Vol. 34, pp. 593~603.

Li, C. and Weng, G. J., 2002, "Antiplane Crack Problem in Functionally Graded Piezoelectric Materials," *Journal of Applied Mechanics, Transactions of ASME*, Vol. 69, pp. 481~488.

Miller, M. K. and Guy, W. T., 1966, "Numerical Inversion of the Laplace Transform by Use of Jacobi Polynomials," *SIAM Journal on Numerical Analysis*, Vol. 3, pp. 624~635.

Shin, J. W. and Kim, T. -U., 2003, "Functionally Graded Piezoelectric Strip with Eccentric Crack under Anti-plane shear," *KSME International Journal*, Vol. 17, pp. 854~859.

Shin, J. W., Kwon, S. M. and Lee, K. Y., 2001a, "Eccentric Crack in a Piezoelectric Strip under Electro-Mechanical Loading," *KSME International Journal*, Vol. 15, pp. 21~25.

Shin, J. W., Kwon, S. M. and Lee, K. Y., 2001b,

"An Eccentric Crack in a Piezoelectric Strip under Anti-plane Shear Impact Loading," *International Journal of Solids and Structures*, Vol. 38, pp. 1483~1494.

Sneddon, I. N., 1972, *The Use of Integral Transforms*, McGraw-Hill Book Company.

Wang, B. L., 2003, "A Mode III Crack in Functionally Graded Piezoelectric Materials," *Mechanics Research Communications*, Vol. 30, pp. 151~159.

Wang, B. L. and Mai, Y.-W., 2003, "On the Electrical Boundary Conditions on the Crack Surfaces in Piezoelectric Ceramics," *International Journal of Engineering Science*, Vol. 41, pp. 633~652.

Xu, X. L. and Rajapakse, R. K. N. D., 2001, "On a Plane Crack in Piezoelectric Solids," *International Journal of Solids and Structures*, Vol. 38, pp. 7643~7658.

Zhang, T.-Y. and Tong, P., 1996, "Fracture Mechanics for Mode III Crack in a Piezoelectric Material," *International Journal of Solids and Structures*, Vol. 33, pp. 343~359.